Chemical characterization of mountain forest soils: impact of long-term atmospheric deposition loadings (Czech–Polish–German border region)

Martina Havelcová, Vladimír Machovič, František Novák, Ladislav Lapčák, Jiří Mizera & Jiří Hendrych

Environmental Science and Pollution Research

ISSN 0944-1344

Environ Sci Pollut Res
DOI 10.1007/s11356-020-08558-x

Springer

Environmental Science and Pollution Research
https://doi.org/10.1007/s11356-020-08558-x

RESEARCH ARTICLE

Chemical characterization of mountain forest soils: impact of long-term atmospheric deposition loadings (Czech–Polish–German border region)

Martina Havelcová[1] · Vladimír Machovič[1,2] · František Novák[3] · Ladislav Lapčák[2] · Jiří Mizera[4] · Jiří Hendrych[2]

Received: 21 October 2019 / Accepted: 23 March 2020

Abstract

The composition of lipids in soil offers clues to soil degradation processes due their persistency and selectivity in soil, and close relation to long-term processes in the ecosystem, thanks to their role in cell membranes of organisms. Organic solvent-extractable compounds were recovered from soils collected at two sites differing in the degree of forest damage. Gas chromatography/mass spectroscopy and Fourier transform infrared spectroscopy were applied in order to characterize solvent-extractable lipids. Raman spectroscopy was also applied as it provides distinct advantages for determining the structural order of carbonaceous materials. The organic matter measurement techniques were combined with an established simultaneous multi-element measurement technique. Variations in individual soil horizons from the sites were reflected in the crystallinity of epicuticular waxes, presence of long-chain aliphatic hydrocarbons, concentrations of *n*-alkanes, saturated and unsaturated fatty acids, dicarboxylic acids, and in the content of aromatic structures, hydroxyl, ester, and carboxylic acid groups. The results are explained by differently transformed organic matter. The concentrations of elements in the soils were also affected by atmospheric depositions, including higher accumulations of arsenic and antimony, and lower contents of natural nutrients. These data have potential to be used as sensitive biogenic indicators of ecosystem damage by long-term atmospheric depositions.

Keywords Soil lipids · Fatty acids · Soil organic matter · Spectroscopy · Chromatography

Introduction

Since the middle of the twentieth century, industrial expansion has generated emissions containing increasingly high levels of sulfur dioxide and nitrogen oxides. Acidic precipitations have become a serious issue across most of Europe, including the Czech Republic. The Czech–Polish–German border region, known as the "Black Triangle," has been severely affected by industrial activities including the extraction of coal resources and power plants. Topography has favored the occurrence of prolonged inversion events, and this led to air contamination, deposition of pollutants, and soil and water acidification (Blažková 1996). Forest stands exposed to acidic clouds and fog resulted in large-scale dieback of spruce trees. In the early 1990s, application of modern technologies, desulfurization of coal power plants, and the use of fuel with low sulfur and nitrogen contents caused a considerable reduction in anthropogenic emissions in the area. There is thus a unique opportunity to compare sets of affected material obtained in 1990s with recently sampled material. The presented investigation is the first step in the aim to see aspects that are related to soil changes in an extremely polluted forest ecosystem after a long-term period of efficient pollution control.

Biochemical processes on a plant's surface vary due to the molecular composition of leaf waxes (Nierop et al. 2005; Hoffmann et al. 2013; Bush and McInerney 2015), and

Responsible Editor: Kitae Baek

Electronic supplementary material The online version of this article (https://doi.org/10.1007/s11356-020-08558-x) contains supplementary material, which is available to authorized users.

✉ Martina Havelcová
havelcova@irsm.cas.cz

[1] Institute of Rock Structure and Mechanics, AS CR V Holešovičkách 41, 182 09 Prague, Czech Republic

[2] University of Chemistry and Technology Prague, Technická 5, 166 28 Prague, Czech Republic

[3] Technopark Kralupy, University of Chemistry and Technology Prague, 278 01 Kralupy nad Vltavou, Czech Republic

[4] Institute of Nuclear Physic, Řež 130, 250 68 Řež, Czech Republic

Published online: 02 April 2020

chemical transformation processes contribute to waxes degradation in soils (Rushdi et al. 2016). Acid deposition and anthropogenic stress caused by emissions from industry or traffic are one of the major global processes that can affect terrestrial biogeochemical cycles and hence plant primary productivity, plant root biomass allocation and associated microbial decomposition. And thereby the composition of soil matter is modified (Norby and Luo 2004; Drissner et al. 2007; Gleixner 2013).

Soil is the largest terrestrial pool of organic carbon, composed of an admixture of a mineral phase and organic matter originating from remnants of plants, animals, and microorganisms at different stages of decomposition and with highly diverse structures. The essential components of plants, and hence of soil, are lipids. In general, plant lipids include derivatives of fatty acids, aromatic and hydrocarbon-like compounds (sterols, carotenoids, and terpenes), and waxes. The solvent-extractable lipids account for up to 10% of the total soil organic carbon (Riederer et al. 1993; Otto et al. 2005; Christie and Han 2010). The content and distribution of lipids in soil organic matter is dependent on the type of overlying vegetation and its characteristic molecular properties (Wiesenberg et al. 2005; Jansen and Wiesenberg 2017; Li et al. 2018). Lipids are interesting in this context because this fraction of soil organic matter (i) is relatively persistent in soil, (ii) is readily and selectively extractable, (iii) is analyzable by instrumental methods, (iv) can vary in chemical composition, and (v) is in close relation with long-term processes in the ecosystem due to roles of lipids in cell membranes of organisms.

Solvent-extractable lipids are a heterogenous group of compounds that include alkanes, alcohols, and carboxylic acids (fatty, dicarboxylic, diterpenoid, hydroxy, free or ester linked) (Graber and Tsechansky 2010). Comparing a number of studies, molecular proxies deriving from solvent-extractable lipids have been assessed using *n*-alkane and *n*-fatty in soils (Maffei et al. 2004; Schäfer et al. 2016; Jansen and Wiesenberg 2017). Several indicators and compound ratios have been developed to assess sources of organic matter and degradation: total lipid concentration carbon preference index (CPI), odd-over-even predominance for *n*-alkanes, and even-over-odd predominance for *n*-fatty acids (Bray and Evans 1961; Scalan and Smith 1970; Otto and Simpson 2006; Zech et al. 2009).

Although a number of case studies describe local sources of pollution in the studied area, little is known about how soil carbon responds to environmental changes, and how lipids are preserved and/or degraded within soil. In this study, solvent-extractable lipids obtained from two different profiles were analyzed. Content of elements was also determined in the studied extracts of lipids to check the soil extracts quality based on elements composition and their quantities. One of major anthropogenic contamination of heavy metal in the environment is fossil fuel combustion, and the investigation provides other useful information on the soil pollution. We studied whether solvent lipids in soil horizons could be used to distinguish between two sites differing in the degree of forest damage. The aims of this paper were (a) to study the molecular composition of lipids as plant input tracers; (b) to determine the impact of anthropogenic pollution on compound composition; (c) to supplement organic compound profiles with the distribution of trace elements; (d) to evaluate the results as possible biogenic indicator parameters of forest ecosystem damage resulting in the death of part of trees, change of vegetation cover, waterlogging of the site with subsequent changes in soil profile.

Material and methods

Site description and soil sampling

Two neighboring study sites Alžbětínka and Mumlavská hora, differing in the degree of forest damage, were located in the western part of The Giant Mountains National Park (Fig. 1). The Giant Mountains form the north-eastern part of the "Black Triangle" border region, affected by the destruction of forest ecosystems by high levels of pollution (e.g., sulfur deposition in 1985 was >2500 mg m^{-1} a^{-1}) (Kolář et al., 2015). The higher levels and persistent occurrence of pollution led to acid deposition (from both sulfur and nitrogen compounds) and extensive forest decline increased sharply after approximately 1960 until the 1990s (Vávrová et al. 2009), with most damage occurring in high-elevation conifer ecosystems. Norway spruce (*Picea abies*) stand canopy cover was in the year 1996 35% (Alžbětínka) and 5% (Mumlavská hora), respectively (Chumanová-Vávrová et al., 2015). Ground vegetation development shifted from prevailing mosses and vegetation-free sites covered with spruce litter to dominance by *Avenella flexuosa* during the earlier period of massive spruce decline. Significant reduction of sulfur deposition (from 50–80 to 26–36 kg ha^{-1} $year^{-1}$) occurred between years 1994 and 1996. Less pronounced decrease followed between 1998 and 2000 (from 30–35 to 6–10 kg ha^{-1} $year^{-1}$) (Vacek et al., 2013). This reduction of immissions has resulted in interruption of the large-scale dieback of spruce stands and has allowed slow regeneration of surviving trees which resulted in a shift in ground vegetation composition (Vávrová et al. 2009).

The Mumlavská hora stand (50° 47′ 45″ N, 15° 28′ 11″ E, 1190 m a.s.l., bedrock granite, stand age 180 years) is located on the mountain ridge; the spruce forest, heavily damaged by acid rain before the end of the twentieth century (Drda, 1994), is represented by a limited number of Norway spruce trees (only 3% of spruce trees survived); plant cover is dominated by purple moor grass and blueberry (*Molinia caerulea*, *Vaccinium myrtillus*, and *Sphagnum* spp.). Gleyed, humic,

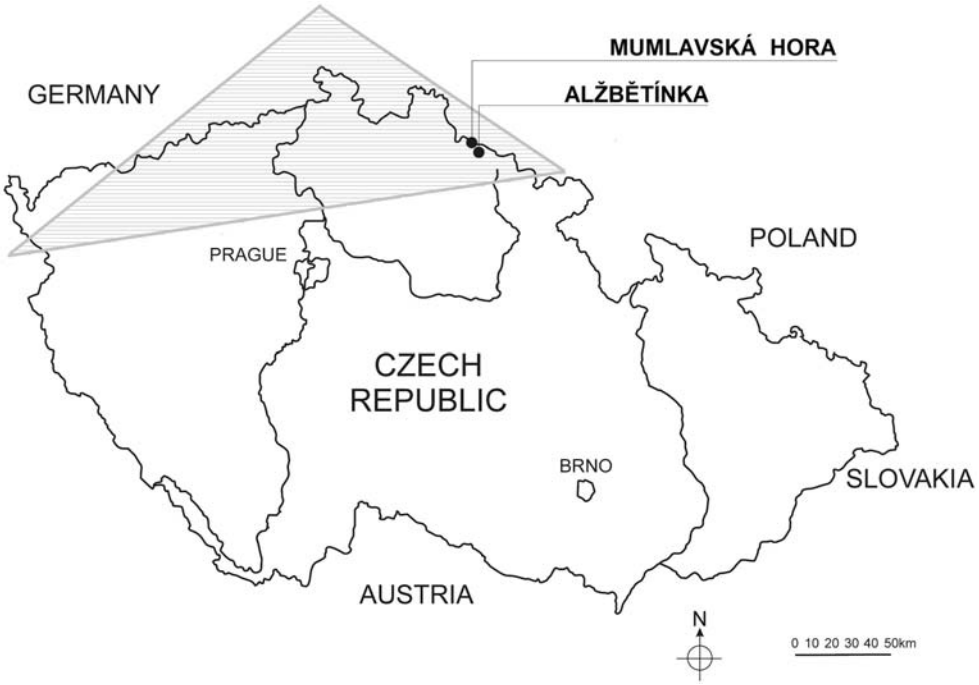

Fig. 1 Location of the Mumlavská hora and Alžbětínka study sites on the edge of the Black triangle area

and histic podzols prevailed on the compact coarse-grained granite, shallow organosol appeared sparsely.

The forest cover in the nearby Alžbětínka stand (50° 45′ 35″ N, 15° 31′ 21″ E, 1220 m a.s.l. bedrock granite, stand age 200 years) is relatively well-preserved (with 46% of living trees). The vegetation cover was dominated by *Picea abies*, *Deschampsia flexuosa*, *Athyrium distentifolium*, and *Calamagrostis villosa*. Soil characteristics are given in Table 1. Podzol soil types (peat, gleyed) developed on the deluvium from granite bedrock occur in the Alžbětínka stand, where soil characteristics are little affected by forest decline. There was no intense peat formation nor waterlogging, in contrast to Mumlavská hora where waterlogging was caused by reduced evapotranspiration and reduced evaporation of precipitation catched on the surface of spruce needles.

The biogeographic conditions at the studied stands, termed arctic–alpine tundra, are characterized by frequent weather changes and long, extremely cold, and damp winters with abundant snow cover (Hejcman et al., 2006). The lowest mean temperatures are observed in January, and the warmest months are June and August. Mean annual precipitation sum is 1340 (Alžbětínka) and 1420 mm (Mumlavská hora), respectively. The highest precipitation occurs in July and the lowest in spring. A continuous snow cover persists from November to

Table 1 Basic characteristics of soils and soil extracts. Base saturation (BS); total organic carbon content in soil (TOC); pH of soil (soil:water ratio 1:5); extracted organic matter in dry soil (EOM); content of elements in extracts (C, H, N, S, O)

	Sample	Soil horizon	Depth (m)	BS (%)	Soil TOC (%)	pH (H_2O)	EOM (%)	%C[a]	%H[a]	%N[a]	%S[a]	%O[a]
Alžbětínka	A1	O_l	0.00 - 0.01		44.1	–	5.24	70.2	8.6	1.0	0.2	20.0
	A2	O_f	0.01–0.08	19	41.9	3.4	4.66	69.2	8.5	1.1	0.2	21.0
	A3	O_h	0.08–0.20	16	3.1	3.3	4.01	70.8	9.1	0.7	0.2	19.2
	A4	A/E	0.20–0.25	9	3.8	4.0	0.28	70.2	9.4	0.8	0.1	19.5
	A5	E(A)	0.25–0.40	6	1.7	4.6	0.26	71.0	9.2	0.8	0.1	18.9
	A6	$B_{sh/s}$	0.40–0.72	15	0.7	4.7	0.07	68.8	9.2	1.2	0.1	20.7
Mumlavská Hora	H1	O_f	0.03–0.08		43.8	4.0	3.75	71.4	9.3	0.8	0.2	18.3
	H2	O_m	0.08–0.15	12	31.2	3.8	4.07	72.6	9.0	0.8	0.2	17.4
	H3	O_h	0.15–0.30	6	2.1	3.7	4.38	72.5	10.2	0.6	0.2	16.5
	H4	E	0.45–0.55	4	3.3	4.3	0.11	71.9	9.9	0.5	0.1	17.6
	H5	(E)/B	0.55–0.65	7	1.3	4.4	0.09	74.4	9.6	0.7	0.1	15.2
	H6	B_{sh}/B_s	0.85	12	0.8	4.5	0.04	74.5	10.5	0.8	0.1	14.1

[a] Dry basis

the beginning of May, and the mean snowpack thickness reaches of approx. 1.8 m. The main ridge is strongly exposed to winds, blowing predominantly from the west or southwest (Kolář et al., 2015). At both locations, the soil moisture regime is humid and the temperature regime is cold. The mean annual air concentration of SO_2 on stands in 1991 was 30 (Mumlavská hora) and 26 μg m^{-3} (Alžbětínka), respectively (Peter et al. 2008). The more damaged Mumlavská hora stand had a lower base saturation of the upper soil horizons and was more influenced by acid rain than Alžbětínka site. Other descriptions of the studied stands were presented by Peter et al. (2008).

Soil samplings were performed in the year 1996 (Mumlavská hora) and 1998 (Alžbětínka). A soil pit (0.8 m L × 0.5 m W × 1.2 m D) was dug at the Mumlavská hora and Alžbětínka stands, and samples were taken from: the organic horizons (O) (litter (O_l), fermentation horizon (O_f), humus (O_h), and mesic (O_m); from the surface humic horizon (A); from the eluvial horizon (E); the subsurface horizon (B) (with accumulation of translocated simple organic compounds, B_h); aluminum or iron (B_{sh}). The soil horizons were distinguished according to the presence of diagnostic properties (Shoeneberger et al. 2002; IUSS Working Group WRB 2007). Samples were air dried at room temperature for approximately 14 days, thoroughly mixed, sieved (< 2 mm), and stored at 0 °C.

Lipid extraction and analysis

Soil pH (in water) and Ca, Mg, K, and Na (extracted with 1 M-ammonium acetate and determined by atomic absorption spectrophotometry) were determined (Miller et al., 2013). Base saturation (BS) (the percentage of the soil exchange sites occupied by basic cations) was calculated as the sum of exchangeable Ca, Mg, K, and Na. Total organic carbon (TOC) determination of ground soil samples was performed by removing inorganic carbon using hydrochloric acid at an elevated temperature and subsequent quantitative carbon determination.

Soxhlet extraction of soils was carried out for 8 h with a mixture of ethanol:benzene 1:1 (v/v) using Whatman cellulose thimbles with 100 g of soil. Extracts were concentrated, dried and used for gas chromatographic/mass spectrometric (GC/MS) analysis (Locatelli et al., 2019; Peters et al., 2005).

For GC/MS analysis, extracts were methylated with boron trifluoride (14% in methanol) (Harmanescu 2012). Esterification was carried out at 70 °C for 3 h. The lipid organic phase was separated and analyzed. Lipid constituents were identified as methyl esters using a Trace Ultra - DSQ II (ThermoScientific, USA) instrument equipped with a capillary column and a fixed stationary phase DB 5 (30 m × 0.25 mm × 0.25 μm film). The GC oven was heated from 37 °C (3 min) to 100 °C at a rate of 10 °C min^{-1} and then to 300 °C (8 min) at a rate of 10 °C min^{-1}. Helium was used as the carrier gas. Mass spectra were recorded at EI 70 eV from 40 to 500 amu in full scan mode. Chromatograms and mass spectra were evaluated using the Xcalibur software (ThermoElectron, UK). Identification of organic compounds was based on comparison of spectra with those from the National Institute of Standards and Technology mass spectral library. The quality of soil organic matter was assessed by the geochemical ratio CPI based on the content of *n*-alkanes in the extracts: $CPI = [(n\text{-}C_{25+27+29+31+33})/(n\text{-}C_{24+26+28+30+32}) + (n\text{-}C_{25+27+29+31+33})/(n\text{-}C_{26+28+30+32+34})]/2$ (Bray and Evans, 1961).

Attenuated total reflection Fourier transform infrared (ATR-FTIR) spectra of bulk lipids were collected on a Nicolet 6700 FTIR (Thermo Nicolet Instruments Co., USA) with a N_2 purging system. Spectra were acquired using a single reflection ATR Pike Technologies GladiATR accessory equipped with a single-bounce diamond crystal (angle of incidence 45°). A total of 64 scans were averaged for each sample and the resolution was 2 cm^{-1}. The spectra were rationed against a single-beam spectrum of the clean ATR crystal and converted into absorbance units by ATR correction. Data were collected in the range 4000–400 cm^{-1}. Due to the fact that the spectra differed mainly in intensities of some bands, some structural semi-quantitative parameters were calculated: ratio I_{2917}/I_{2955} was used to determine the length of the aliphatic chains using band intensities of methylene and methyl groups, ratio I_{1512}/I_{2917} was used to specify aromaticity, ratio I_{3345}/I_{2917} was applied to determine the relative proportion of hydroxyl groups, and the content of ester C=O bonds (I_{1735}/I_{2917}) and carboxyl groups (I_{1711}/I_{2917}) was also estimated (Lin and Ritz 1993; Coward 2010). FTIR (and Raman) spectroscopy proved the presence of methyl and methylene groups of long aliphatic chains, and the splitting of the CH_2 scissoring and rocking modes was indicative of an orthorhombic crystal structure of the hydrocarbon chains. The parameter I_{730}/I_{720}, using the area of bands at 730 and 720 cm^{-1}, was designed to determine the crystallinity (the degree of structural order) of plant epicuticular waxes (LeRoux 1969).

Fourier transform Raman (FT-Raman) spectra were obtained using the Nicolet 9600 spectrometer with the Nicolet Raman module 32B (Madison, WI) and HeNe laser with a maximum power of 2.0 W. The system was equipped with an InGaAs (Indium-Gallium Arsenide) detector, a CaF_2 beam-splitter and a fully motorized sample position adjustment feature. The very low laser output power of 0.01–0.5 W used for analysis was low enough to prevent possible laser induced sample damage yet provided a high signal-to-noise ratio. Data were collected at 4 cm^{-1} resolution with 1024 scans. Spectra were obtained in the Raman shift range between 400 and 3700 cm^{-1}. The system was operated using OMNIC software (Version 9.2, Thermo Fisher Scientific).

The elemental composition of bulk lipids was determined using a carbon, hydrogen, nitrogen, sulfur micro-analyzer (Thermo Finnigan Flash EA 1112, Italy). Other elements of bulk lipids were assayed by instrumental neutron activation analyses (INAA). Irradiations for INAA were carried out in the LVR-15 experimental nuclear reactor of the Řež Research Centre. A detailed description of the analytical procedures can be found in Mizera and Řanda (2010).

Quality assurance

Blank extraction samples, duplicate samples, and certified reference materials were processed along with the samples. Solvents of pesticide grade were purchased from Analytika (Prague, Czech Republic).

Repeated acquisitions on the crystals using the highest magnification (× 50) were accumulated to improve the signal to noise ratio of the Raman spectra. FTIR spectra were processed with ATR correction. All molecular markers in GC/MS were identified by retention times and the mass spectral quantification ions of detected compounds. To quantify these compounds, a solution of 5α(H)-androstane (Dr. Ehrenstorfer GmbH, Augsburg, Germany) in dichloromethane was added as an internal standard.

To evaluate the precision of the analysis, three replicates of samples were analyzed, and the standard deviations of the replicates were calculated (Supplementary Material S1). In assessing repeatability (precision), the relative standard deviation for certified reference soil material METRANAL9 (Analytika, Prague, Czech Republic) was shown to be in the range 1.8–6.4%.

The accuracy of the INAA measurements was tested by analysis of certified reference materials (NIST Standard Reference Materials), namely SRM-2711Montana Soil (deviation <10 rel.%). The principal component analysis—multivariate statistical analysis method—was applied on total element values for soil samples using the Statistica 10.0 package software, to evaluate the samples and to illustrate element sources.

Results

Total organic carbon (TOC) in soil samples ranged from 44% in the top-soil to 1% in the subsurface horizons (Table 1). A significant decrease in TOC was observed between the O-horizons and the A/E horizons for both sites with an additional decrease observed for the E/B boundary, which may have been due to a decrease in the number of roots (Naafs et al. 2004). The pH values of both soils were acidic throughout the horizons, ranging from 3.3 to 4.7, which have been caused by several influences: high elevation area, forest soils, and the effect of lignite mining and burning of materials containing pyritic components (iron and sulfur or sulfur oxides). High precipitation also can cause leaching of base-forming cations and the lowering of soil pH (McCauley et al. 2017). The acidic character of soil horizons was in agreement with the low base saturation in soil (Table 1) when the acidic cations adsorbed on the negatively charged surfaces of soil clay and organic particles caused deprivation of non-acid cations (Ca^{2+}, Mg^{2+}, K^{+}, Na^{+}).

The greatest contribution of extractable organic matter to TOC was revealed in O_h (Table 1) and can be explained by an input of organic compounds from litter layers and advanced decomposition of humic material. The decrease in lower horizons was due to selective biodegradation of organic compounds from litter layers and their lower input from roots, connected with lipid transfer into macromolecular and organo-mineral complexes.

In the soil extracts (EOM), the carbon contents were high and the other elemental composition of organic matter differed only slightly within profiles. Elements Na, K, As, Sb, Fe, Se, Co, and Zn were also identified in the organic extracts. The principal component analysis, using total element concentrations of the both stands, revealed that 76.7% of the dispersed variable could be assigned to two factors (Fig. 2): factor 1 groups Na, K, Fe, and Co; factor 2 groups Se, As, and Sb with positive loadings, and Zn with negative loadings. This indicates that the distribution of the elements in organic extracts is affected by their sources, eluviation/illuviation and bioavailability (Beone et al. 2018).

FT-Raman spectroscopy was applied to total lipid extracts so as to determine the structural order of carbonaceous materials (Parikh et al. 2014). However, spectra of soil extracts showed significant fluorescence, mainly in extracts from the upper organic O-horizons having the strongest biological trace (high content of organic matter). Prominent intense features between 3000 and 2800 cm^{-1} (not shown) can be assigned to

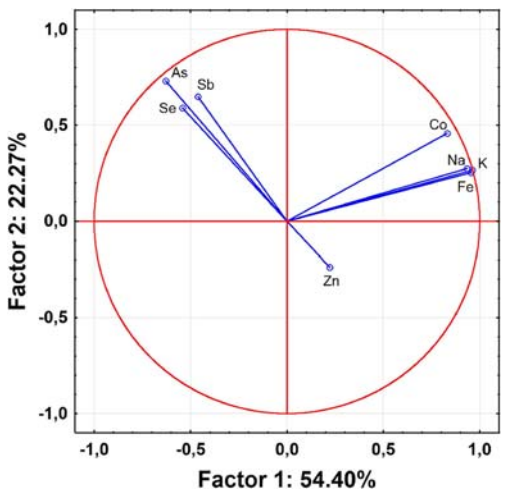

Fig. 2 Principal component analysis for the soil extracts. Total element concentrations of the both stands were used

vibrations of aliphatic C-H bonds. The spectral region 1800–600 cm^{-1} was dominated by an intense sharp peak at 1295 cm^{-1} belonging to deformation twisting vibrations of methylene groups in structures with long aliphatic chains (Fig. 3a, Table 2). Aliphatic structures were also confirmed by the deformation vibrational bands $\delta(CH_2)$ at 1460, 1439, and 1418 cm^{-1}. A triplet at 1124, 1083, and 1062 cm^{-1} belonged to the stretching vibration of C-C bonds. The presence of aromatic structures was shown by bands of weak intensity at 1630 and 1605 cm^{-1} belonging to the stretching vibrations of C-C bonds in aromatic rings. A broad and complex feature at 890 cm^{-1}, consisting of three bands at 914, 891, and 867 cm^{-1}, could belong to the stretching vibrations ν(C-C) and ν(CCO); however, in this region, bands of plane C-H vibrations in aromatic structures could also be represented. A small band at 1365 cm^{-1} was one of antisymmetric deformation vibrations of methylene groups. The presence of carbonyl groups in esters showed a band of very low intensity at 1742 cm^{-1}.

In the ATR-FTIR spectra of bulk lipid extracts, sharp intense stretching vibrational bands of C-H bonds dominated in the region 3000–2800 cm^{-1}, similar to the Raman spectra. Using the second derivative and curve-fitting of the spectra, seven bands that were due to vibrations of the methyl, methylene and methine groups, and methoxy groups were found (Fig. 3b, Table 2). The deformation vibrations of aliphatic C-H bonds were represented by intense deformation doublets of scissor vibration and rocking at 1472/1464 cm^{-1} and 730/720 cm^{-1}. The band at 1415 cm^{-1} belonged to the deformation vibration of a methylene group adjacent to a carboxyl group. A slightly intense band at 1378 cm^{-1} (Fig. 3b) was attributed to the symmetric deformational vibration of methyl groups. In the spectral region 1345–1180 cm^{-1}, a number of bands of relatively low intensity were found, having a periodicity value at the peak position. This series of bands is usually observed in the infrared spectra of long-chain fatty acids and their esters. The number of carbons in the long chains of these compounds is equal to half of the bands in their infrared spectra. The term "band progression" was applied to such a series of bands (Swalen et al., 1987). Jones et al. (1952) showed that these bands were attributable to the CH_2 wagging and/or twisting modes. Unfortunately, however, in this spectral region, bands ν(C-O) can also be found, making it difficult to interpret infrared spectra of such a complex mixture of compounds. A clearly distinguishable band at 1514 cm^{-1} and two less resolved bands at 1630 and 1605 cm^{-1} were ascribed to stretching vibrations of C-C bonds in aromatic rings, and are indicative of the presence of phenolic compounds in the extracts. Broad bands around 3400 and 3266 cm^{-1} were assigned to the stretching vibration of O-H and N-H groups that interact by H bonding. The intensities of these bands are known to be depended on the plant species (Heredia-Guerrero et al. 2014). Two intense sharp bands at 1734 and 1711 cm^{-1}, found in the spectra, belonged to the stretching vibrations of carbonyl bonds in esters and carboxylic acid groups.

Using GC/MS, the distribution of *n*-alkanes (*n*-C_{21} to *n*-C_{31}) reflected the predominance of odd-over-even carbon atom number with C_{max} mainly at 29 and/or 31. The *n*-alkane distribution was the same for all sample extracts from both stands, however, their content was higher in extracts of soils from upper parts of Mumlavská hora. Free fatty acids (FAs) were identified in the extracts, ranging from *n*-dodecanoic acid (12:0) to *n*-tetracosanoic acid (24:0). Saturated compounds dominated in the distribution record, but unsaturated FAs (16:1) were also found, as well as straight-chain C_{14}-C_{18} *n*-alkanoic acids. The most distinct feature of the fatty acid distribution was the predominance of compounds with an even number of atoms in a molecule and dominance in hexadecanoic and docosanoic acids. Vanillic acid (4-hydroxy-3-methoxybenzoic acid) was the most intensive of the dihydroxybenzoic acids, next to dihydroxydimethylbenzoic acid. Terpenoids, plant biomarkers, were also identified in extracts: longifolen, lambda-8(20),14-dien-13-ol and dehydroabietic acid, which are also often classified amongst lipids. Their content with depth declined as well as the content of alcohols (phytol) and sterols (stigmasterol).

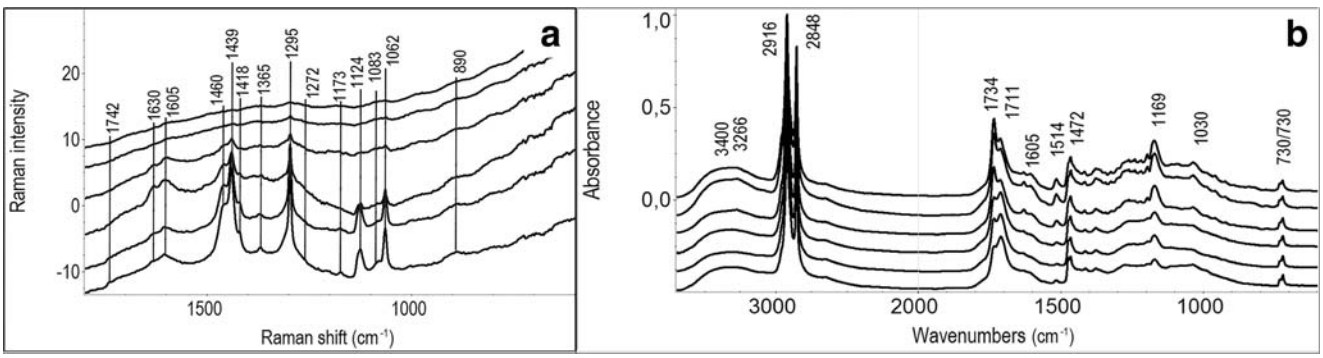

Fig. 3 **a** Raman spectra of soil extracts from the Mumlavská hora stand. **b** Infrared spectra of extracts separated from the Alžbětínka stand. Spectra were sorted by the soil horizon from top to bottom

Table 2 Assignment of vibrational modes for the FT-Raman and for the FTIR spectra. (Zerbi et al. 1981; Edwards et al. 1996; Neubert et al. 1997; Lu et al. 1998; Merk et al., 1998; Dubis et al. 1999; Beattie et al. 2004; Movasaghi et al. 2008; Coward 2010; Heredia-Guerrero et al. 2014)

FT-Raman spectra		FTIR spectra	
Band (cm^{-1})	Assignments	Band (cm^{-1})	Assignment
2963*, 2929*, 2902*	$\nu_{as}(CH_3)$	3440–3360	ν(O-H)
2881*	$\nu_{as}(CH_2)$	3266	ν(N-H)
2850*	$\nu_s(CH_2)$	2955*	$\nu_{as}(CH_3)$
1742	ν(C=O) esters	2930*, 2917*	$\nu_{as}(CH_2)$
1630, 1605	$\nu(C\text{-}C)_{ar}$	2898*, 2870*	$\nu_s(CH_3)$
1460, 1439	$\delta(CH_2)$ scissoring	2849*	$\nu_s(CH_2)$
1365	$\delta(CH_2)$ wagging and twisting	2830*	$\nu_s(OCH_3)$ methoxy
1306, 1295	$\delta(CH_2)$ twisting	1734	ν(C=O) esters
1272, 1255	$\delta(=CH)_{ip}$ olefinic hydrogen bend	1711	ν(C=O) in COOH
1203	ν(C-C)	1688	ν(C=O) in COOH
1173	$\rho(CH_2)$	1650	Protein amide II
1133, 1124	ν_s(C-C)	1630, 1605, 1514, 1478	$\nu(C\text{-}C)_{ar}$
1083	ν(C-C), chain with g units	1550	Protein amide II
1062	ν_{as}(C-C)	1472/1464	$\delta_s(CH_2)$ scissoring
1065–1060	ν(C–C) out-of-phase aliphatic all-trans	1437	$\nu(C\text{-}C)_{ar}$, ν(C-O), δ(OH)
1050	$\delta(CH_2)$ twisting	1415	$\delta(CH_2)$ adjacent to COOH
1033,1000	$\nu(CC)_{ar}$ ring breathing	1378	$\delta(CH_3)$ umbrella
975, 957	$\rho(CH_3)$	1342, 1325, 1311, 1301, 1280, 1272, 1251, 1248, 1238,1223, 1217, 1205, 1194, 1177, 1169	$\delta(CH_2)$ wagging + twisting, ν(C-O) esters
914	ν_s(C-C) head	1089, 1062, 1030, 1016	ν(C-C), ν(C-O) alcohols
891	$\rho(CH_3)$ chain-end tt	955	γ(COH) acids
920–800	$\nu(C_1\text{–}C_2)$, $\rho(CH_3)$, ν(C–O)	883, 831, 778, 744	$\gamma(C\text{-}H)_{ar}$
725	ν(CC)	730/720	$\rho(CH_2)$

Notation of vibrational modes: ν, stretching; δ, bending; γ, out-of-plane; ρ, rocking; s, symmetric; a, asymmetric; ar, aromatic; ip, in-plane

*Band positions were determined by second derivative and curve fitting

Discussion

Alžbětínka

The concentrations of *n*-alkanes (Fig. 4A), fatty acids (Fig. 4D, E, F, Supplementary Material S1), as well as the content of carboxyl groups, as determined by ATR-FTIR (Fig. 5C), were highest in the upper O-horizons and decreased in the lower horizons. Such a distribution agrees with the natural situation where fresh plant materials are stored in O-horizons at various stages of decomposition.

The saturated FAs identified yielded a strong even predominance originating from vascular plants ($C_{18:0}$-$C_{25:0}$), bacteria, and other soil microorganisms ($C_{12:0}$-$C_{18:0}$). The O_l topsoil horizon comprises the source of *n*-alkanes and FAs from epicuticular waxes of vascular plants. With time, and mixing of the mineral matter in soil, the compounds concentrate in the O_h-layer (Fig. 4A). *n*-Alkanes naturally occur in the waxy coating of plant leaves but it is known that they are also formed from FAs, either directly by decarboxylation or by condensation between two biochemically dissimilar FAs followed by specific decarboxylation of one of them (Kolattukudy 1970). The increase in *n*-alkanes in the O_h-horizons could largely be due to degradation, mainly in relation to decreasing concentrations of saturated and unsaturated FAs (Fig. 4D, E). The ratio of long-chain FAs and short-chain FAs (FA > 18/FA < 18) was applied to identify variations in the contribution of vascular plants, bacteria and other soil microorganisms for the saturated fatty acids. Their significant decrease of FAs in the lower-horizons is the result of limited transport of these compounds into the mineral horizons, reduced input and microbial degradation, a process proven by the lowering of FA > 18/FA < 18 ratios (Fig. 4C). This ratio of acid content with carbon number over 18 to those below 18 indicates a microbial presence in proportion to the plant source. The higher concentrations of saturated and unsaturated acids in the O_f horizon supports the assumption of higher microbial activity and a contribution from root biomass (Simoneit 2005). The concentration of dicarboxylic acids was highest in the O_h-horizon of overlying humus. Such an

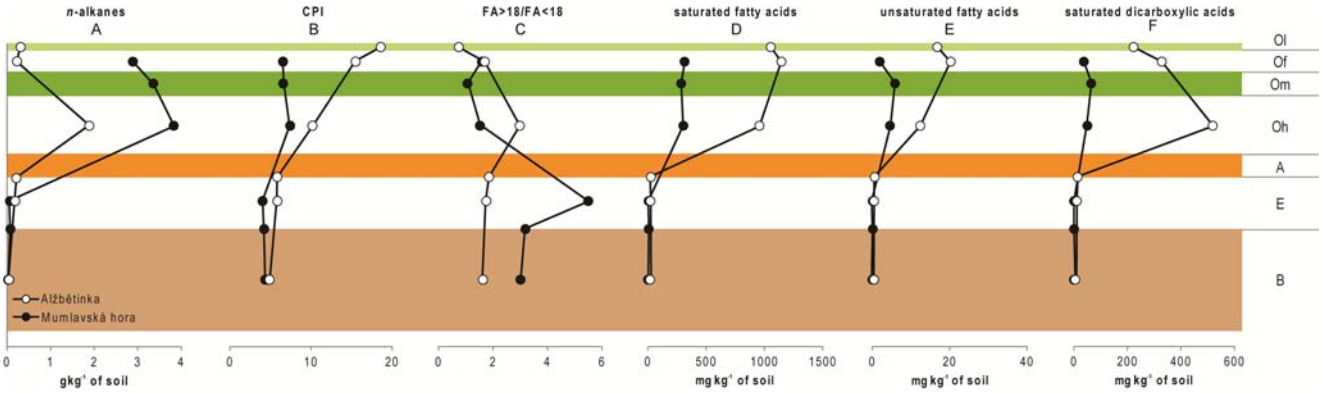

Fig. 4 GC/MS results: (A) contents of n-alkanes; (B) carbon preference indices showing the ratio of odd-to-even predominance in n-alkane distribution (CPI); (C) ratios of acid contents with carbon number over 18 and acids having a carbon number below 18; (D) saturated fatty acids, (E) unsaturated fatty acids, and (F) saturated dicarboxylic acids in the horizons studied

increase can be rationalized as the hydrolyzed products of unsaturated alkanoic and hydroxy acids, components of the epidermis and periderm (suberin and cutin) (Nierop et al. 2005; Otto and Simpson 2006; Rushdi et al. 2016).

The content of aromatic structures (I_{1512}/I_{2917}) in the extracts had an analogous record throughout the profile: higher in upper O-horizons and reducing with depth, as shown by infrared spectroscopy (Fig. 5B). Aromatic acids are secondary plant metabolites and degradation products of phenolic polymers and monomers after decomposition of suberin and ligno-cellulose complexes of plants (Gallet and Keller 1999). The content of hydroxylic, ester and carboxylic acid groups (Fig. 5C, D, F) showed that there was a noticable relationship between the content of hydroxyl groups and aromaticity (Fig. 5B), supporting the concept of collocation of phenolic and aromatic compounds and ongoing degradative processes. Otto and Simpson (2006) also observed phenolic compounds vanillin, vanillic acid, syringic acid, and p-coumaric acid in samples of the pine forest soil, that were again interpreted as being predominantly derived from suberin, with an additional input from the ligno-cellulose complex. For example, the concentration of aromatic vanillic acid, which is a microbial degradation product of lignin or ferulic acid (Mäkelä et al. 2015), was 18 ng mg^{-1} at the O_f-horizon, and decreased to 0.7 ng mg^{-1} in O_h, and to zero in $B_{sh/s}$.

The relative proportion of long aliphatic chains (I_{2917}/I_{2955}) showed a tendency to increase with depth (Fig. 5E) which seems to be associated with a decrease in ester group signals (I_{1735}/I_{2917}) (Fig. 5D). There are several possible explanations: (a) long-chain acids had a lower abundance in leaves and higher in roots and stems (Wiesenberg et al. 2005); (b) during degradation of plant biomass, long-chain carbohydrates were selectively preserved in soils as the short-chains were decomposable by soil microbes (Ussiri and Johnson 2003); (c) microorganisms are known to synthesize alkyl carbohydrate structures as metabolic products of decomposition, and the decrease in methoxy (ester) groups (Fig. 5D) could be attributed to this biological degradation of relevant hydrocarbons (Hatcher et al. 1983; Kögel-Knabner 2000).

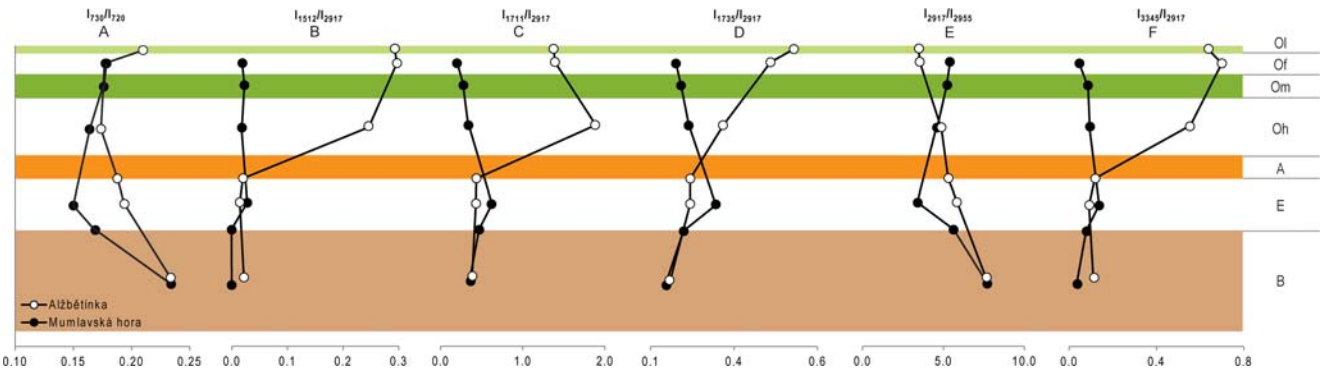

Fig. 5 Structural semi-quantitative parameters obtained from FTIR results: (A) crystallinity based on CH_2 scissoring and rocking modes (I_{730}/I_{720}); (B) relative representation of the aromatic structures based on the ratio of band intensities, aromatic-ring vibrations, and deformation vibrations of methylene (I_{1512}/I_{2917}); (C) carboxyl groups representations (I_{1711}/I_{2917}); (D) ester content representations (I_{1735}/I_{2917}); (E) aliphatic chain lengths based on the ratio of band intensities of aliphatic C-H bonds in methylene and methyl groups (I_{2917}/I_{2955}); (F) hydroxyl group representations based on the intensities of the band at 3345 cm^{-1} and the band of methylene groups at 2955 cm^{-1} (I_{3345}/I_{2955}) in the horizons studied

The quality of soil organic matter, assessed by the CPI ratio, utilizes the fact that for terrestrial plants, the odd-over-even superiority for the *n*-C_{24} to *n*-C_{34} homologs is characteristic and vanishes with plant decomposition. High CPI values (Fig. 4B), typical for matter dominated by terrestrial vascular plants, were observed in the upper horizons, and lowering of values indicates the degradation of organic matter biomass (Cranwell 1981; Gocke et al. 2014).

The values of crystallinity (I_{730}/I_{720}) (Fig. 5A) showed that the aliphatic crystalline was well ordered in the upper O_l part of the soil, full of fresh plant litter, as a high degree of crystallinity is usual for plant epicuticular wax (Merk et al. 1998; Koch and Ensikat 2008). Waxes progressed through decomposition in the other parts of the O-horizon but in the A horizon, values increased again. This suggests that the wax morphologies had a crystalline structure again, probably through a self-assembly process, in which molecules interacted and formed well-defined humic structures. Environmental factors (temperature, substrate might) could have influenced this self-assembly process, as was proven under laboratory conditions (Koch and Ensikat 2008).

Members of the terpenoid and steroid groups, derived from conifer waxes, formed only a minor proportion of the extracts and their contents declined with depth. Stigmasterol showed the most striking change in concentration with depth (29 ng mg^{-1} at O_f-horizon, decreased to 8 ng mg^{-1} in O_h and to 8 ng mg^{-1} in $B_{sh/s}$) (Supplementary Material S1). A decrease in steroids has been observed by Naafs et al. (2004) comparing litter layer extracts with those from underlying A-horizons and was explained by compound mineralization, arthropod assimilation or inclusion into the insoluble fraction. Such a decrease between O_f and O_h can also be explained by the incorporation of free compounds into biogenic insoluble macromolecules (Amblès et al. 1991).

Natural element input/output to the soil horizons occurs predominantly via decaying plant materials and the uptake of elements via plant roots from the deeper mineral soil. Elements from the Factor 1 groups, Na, K, Fe, and Co, which are essential plant nutrients, showed corresponding distributions with the highest concentrations being in the extract of soil sampled from the O_f-horizon (Fig. 6). They were concentrated at this horizon as a result of plant decay. In lower horizons, these elements were bonded to humic substances due to the strong binding capacity of humus, or were presented in a mineral matrix with concentrations depending on the sorption capacity of the appropriate horizon.

The input of As, Sb, Se, and Zn into the forest ecosystem seems to be anthropogenic, related to human activity. Arsenic occurs naturally in soils at concentrations ranging from 1 to 40 mg kg^{-1} (Zhou et al. 2017), and antimony at concentrations ranging from 0.05 to 8.8 mg kg^{-1} (Doherty et al. 2017), and the background levels are differentiated by geographic regions and type of soils. For both elements, the highest concentrations in the soil extracts studied were at the O_h-horizon 0.36 and 0.04 mg kg^{-1}, respectively (Fig. 6C, D). Although these values were within the background of the elements, they referred only to a part of element bind to organic matter that was extracted from the soil. The total concentration of As and Sb in soil can be supposed much higher. The main input would be atmospheric deposition that first comes into contact with top humus horizons. Another overlap with organic material is followed by mineralization and physico-chemical processes that result in the occurrence of variously mobile elemental forms. In the lower soil profiles, the elements moved together with the soil solution, which contains soluble complexes and suspended particles. Metal mobility depends on many factors; elements can be adsorbed and transported with humic substances or clay minerals, and soil pH is the main index that influences soil reactions.

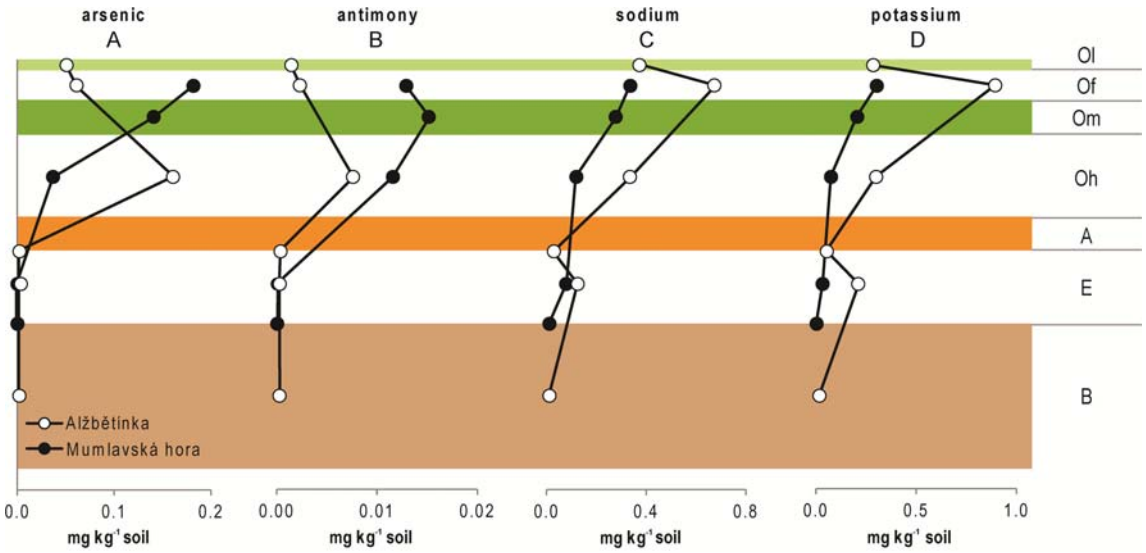

Fig. 6 Results of INNA: Content of (A) arsenic, (B) antimony, (C) sodium, and (D) potassium in the horizons studied

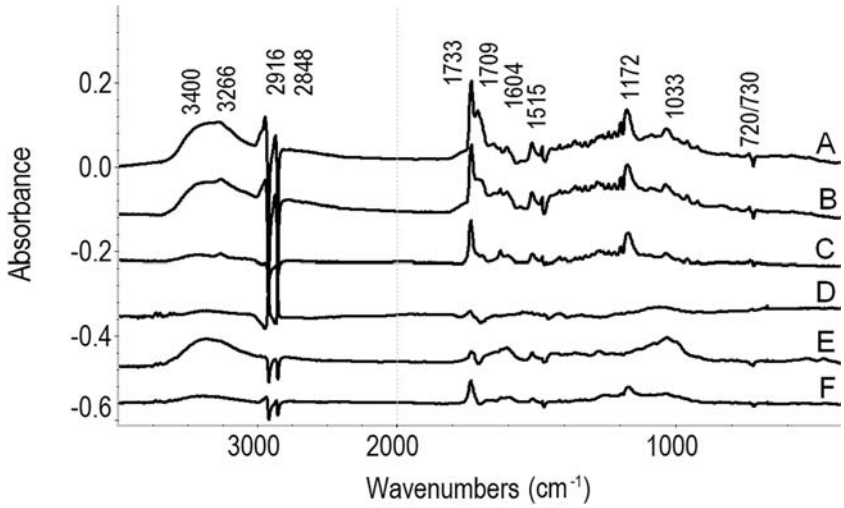

Fig. 7 Difference ATR-FTIR spectra obtained by subtraction of the spectra: (A) A1-H1, (B) A2-H2, (C) A3-H3, (D) A4-H4, (E) A5-H5, (E) A6-H6

The highest concentrations of As and Sb were at the horizon that had the lowest pH. Similar results have been reported by Bissen and Frimmel (2003), who concluded that a more acidic soil promotes As mobilization. The source of Se and Zn can be anthropogenic as well as natural (Imperato et al. 2003; He et al. 2018). Zn had negative loadings in PCA, which may have been caused by its high bioavailability and mobility when the element leaches through the soil (Yelpatyevsky et al. 1995).

Mumlavská hora

Higher concentrations of *n*-alkanes (Fig. 4A) and lower concentrations of *n*-alkanoic acids (Fig. 4D, E, F) compared with Alžbětínka may be derived from the prevailing purple moor grass and blueberries amongst conifers because it is known that conifer leaves synthesize lower amounts of *n*-alkanes and higher amounts of acids in comparison with other terrestrial plants (Bush and McInerney 2013; Diefendorf et al. 2015). Also, the extracts revealed longer aliphatic chains in the topsoil O horizons compared with Alžbětínka (Fig. 5E). Alkane proxy CPI values (Fig. 4B) were similar throughout the profile and low (< 10), indicating degradation of organic matter and root-derived biomass (Gocke et al. 2014). The quantity of long aliphatic chains (I_{2917}/I_{2955}) indicated a tendency to decrease with depth (Fig. 5E). This relative reduction in long chain components in E seems to be caused by preferential degradation of alkanes $>C_{25}$ (Fig. 4B), and selective preservation of hydroxylic, ester and carboxylic acid groups (Fig. 5C, D, F). Such trends could be the result of lower levels of microbial activity that have not been able to cope with decomposable carbohydrates, which also corresponds with the FA > 18/FA < 18 ratio showing higher values matching the limited activity of bacteria and other soil microorganisms in the E-horizon (Fig. 4C). Regardless of the lower *n*-alkanoic acid concentrations (Fig. 4D, E, F, Supplementary Material S1), the distribution included acids with a strong even predominance, originating from vascular plants

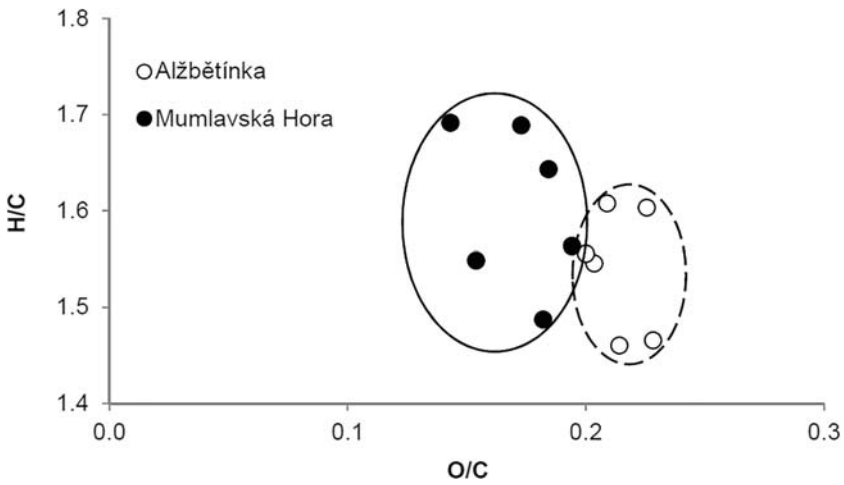

Fig. 8 Van Krevelen diagram: a plot of atomic oxygen/carbon (O/C) versus atomic hydrogen/carbon (H/C) used to predict compositional evolution/turn

($C_{18:0}$-$C_{25:0}$), bacteria and other soil microorganisms ($C_{12:0}$-$C_{18:0}$), and the fatty acids (saturated, unsaturated) and dicarboxylic acids showed a small increase in content in the O_m- or O_h-horizons.

Values of crystallinity were very similar to values found for Alžbětínka in the topsoil O-horizons, but the recovery of crystallinity started deeper from horizon E (Fig. 5A). This could be due to various reasons, but generally, soil crystallinity is largely impacted by environment (pH, soil character, temperature). We hypothesize that the soil with poorly crystalline phases could indicate contaminated conditions. Due to these conditions, self-assembly of wax was affected and was lower in deeper parts of the stand. The relative concentration of OH groups was lower in the topsoil O-horizons compared with extracts from Alžbětínka (Fig. 5F), and the content of ester C=O bonds (I_{1735}/I_{2917}) and carboxyl groups (I_{1711}/I_{2917}) did not change much with the depth profile (Fig. 5C, D).

Effect of pollution

The structures of solvent-extractable lipids from both profiles studied were compared using difference spectra obtained by subtracting one FTIR spectrum (Mumlavská hora) from the other (Alžbětínka) (Fig. 7) obtained for the appropriate horizons to see differences. The resulting spectra revealed a higher oxygen functionality content in extracts of the Alžbětínka profile, as shown by the positive bands at 3400 cm^{-1} (OH), 1735 cm^{-1} (COOR), and 1709 cm^{-1} (COOH). Positive bands at 1630, 1609, 1478, 830, 815, and 730 cm^{-1} showed the presence of aromatic phenolic structures. Protein bands at 3266, 1650, and 1550 cm^{-1} were found in the extracts of three upper organic O-horizons in Alžbětínka. On the other hand, extracts of the Mumlavská hora profile showed a higher content of long aliphatic chain compounds, as evidenced by the presence of sharp intensive methylene bands at 2916 and

Table 3 Basic difference between the stands and groups of compounds identified in the soil extracts

	Alžbětínka		Mumlavská Hora	
GPS	50° 45′ 35″ N 15° 31′ 21″ E		50° 47′ 45″ N 15° 28′ 11″ E	
Altitude	1220 m a.s.l.		1190 m a.s.l.	
Vegetation cover	46% of trees		3% of trees	
H/C range	1.46–1.61		1.49–1.69	
O/C range	0.20–0.23		0.14–0.19	
Sodium (mg kg^{-1} soil of all horizons)	1.55		0.85	
Potassium (mg kg^{-1} soil of all horizons)	1.77		0.63	
Arsenic (mg kg^{-1} soil of all horizons)	0.28		0.36	
Antimony (mg kg^{-1} soil of all horizons)	0.01		0.04	
Compound class	Sum of mg kg^{-1} soil of all horizons		Sum of mg kg^{-1} soil of all horizons	Main source
Fatty acids				
Saturated fatty acids $C_{12–24}$	3157	C_{12}-C_{24}	863	Suberin/cutin
Dicarboxylic acids $C_{10–22}$	1099	C_{15}-C_{22}	155	Suberin/cutin
Branched alkanoic acids $C_{14–22}$	56	C_{14}-C_{20}	58	Bacteria, vascular plants
Unsaturated fatty acids $C_{16–20}$	88	C_{16}, C_{18}	10	Plant seeds
Benzoic acids				
Dihydroxydimethylbenzoic acids	294			Lignin
Vanillic acid	12	Vanillic acid	6	Suberin/cutin
Terpenoids				
Longifolene	52			Resin
Labda-8(20),14-dien-13-ol	655			vVascular plant waxes
Dehydroabietic acid	76			Conifer resin
Phytol	63	Phytol	22	Vascular plant waxes
Steroids				
Cholestadienol	71	Cholestadienol	31	Cholestadienol
Fatty aldehydes				
C_{15}, C_{18}	152	C_{15}	1	Suberin/cutin
n-Alkanes				
C_{21}-C_{31}	2892	C_{21}-C_{31}	10,262	Vascular plant waxes

2848 cm^{-1}. Chemical transformation and the presence/absence of oxygen-rich molecules were also demonstrated by the atomic ratios of H/C and O/C in the extracts. For soil extracts from Mumlavská hora, these values were shifted in the van Krevelen diagram (Fig. 8) to higher H/C and lower O/C ratios in comparison with Alžbětínka extracts. They had higher oxygen and lower carbon contents (Table 1), and this agrees with higher amounts of hydroxyl, carboxyl, esters and carbonyl oxygen-containing groups.

Generally, soil characteristics at the Alžbětínka stand can be considered to be little affected by forest decline: the intensity of long aliphatic chains in the Alžbětínka extracts increased continuously with depth (Fig. 4E), aromaticity and CPI values decreased (Fig. 5B), and correlated with the relative proportion of hydroxyl groups (Fig. 5F). The content of ester C=O bonds and carboxyl groups also decreased with the depth profile (Fig. 5C, D). Conversely, the composition of soil lipids reflected the different situation at Mumlavská hora by displaying an entirely different profile than that of the Alžbětínka stand (Table 3). The extract analysis revealed higher *n*-alkane contents in the upper horizons (Fig. 4A), variable distribution with depth of long aliphatic hydrocarbons (Fig. 5E), and lower CPI values (Fig. 4B), arguing for a different plant source and uncertain degradation. The contents of aromatic structures, hydroxylic, ester and carboxylic acid groups (Fig. 5B, C, D, F) were low in the whole profile and changed slightly with depth, probably reflecting the greater contribution of degraded and microbial biomass in O-horizons. Differences between soil stands were evident in the abundance of all types of fatty acids - saturated, unsaturated, and dicarboxylic acids (Fig. 4D, E, F; Table 3).

Moreover, the lower concentrations of Na and K and higher concentrations of As and Sb (Fig. 6), in comparison with soil extracts from Alžbětínka, are evidence of a more polluted stand at Mumlavská hora. Nitrogen and sulfur emissions from combustion of fossil fuels formed sulfuric and nitric acids (in clouds) and returned to the earth in precipitation and dry deposition. Soil acidification and accumulation of organic carbon from *Molinia caerulea* occurred at Mumlavská hora, accelerating biogenic element losses (Bonifacio et al. 2008). As and Sb speciation analysis can be employed as a geochemical tracer of anthropogenic emissions (Sánchez-Rodas et al. 2017). Lignite mining and burning in the Czech–Polish–German border region have influenced the distribution of these elements. They have accumulated free, mineralized and/or bound due to a tendency to promote organic binding (Reimann et al. 2007; Sucharová et al. 2011). The concentration of these elements was highest in the upper horizons but the values seem to be low in comparison with data given by Sucharová et al. (2011) for forest floor humus - up to 85.8 mg As kg^{-1} soil and 6.5 mg Sb kg^{-1} of soil. But it must be taken into account that the concentrations found could only represent a small proportion of all elements because they were detected in organic extracts.

Conclusion

Transformation of plant litter constituents in soils depends on climate and deposition impacting the physico-chemical conditions of soil, plants, the state and activity of bacteria, and other soil microorganisms. The impact of acid rain and acid deposition causes changes in plant growth and soil pH. Soil acidification reduces the biological activity of soils by limiting both the number of microorganisms and biochemical processes, and inhibits plant matter decomposition processes, as is visible in this study of soil extracts from two differently damaged stands. The samples and their fractions displayed differences in chemical composition. Extracts of the more damaged stand Mumlavská hora showed a lower content of fatty and benzoic acids, terpenoids, and steroids, and a higher content of *n*-alkanes, arsenic and antimony. Under more favorable conditions at the Alžbětínka stand, features included higher amounts of oxygen-containing groups with lower turnover rates, plant fatty acids and aromatic structures with longer life times, supporting crystalline order, prevailing longer aliphatic chains. Acid rain and incidental forest decline affected the processes in soil biomass, and similar features were not recognizable in samples from Mumlavská hora.

Acknowledgments This work was carried out thanks to the Operational Program Prague—Competitiveness, project "Centre for Texture Analysis" (No. CZ.2.16/3.1.00/21538). The financial support provided by the long-term conceptual development of research organization RVO: 67985891 is also gratefully acknowledged. The authors are grateful to John Brooker for reviewing and correcting the manuscript.

References

Amblès A, Jacquesy JC, Jambu P, Joffre J, Maggi-Churin R (1991) Polar lipid fraction in soil: a kerogen-like matter. Org Geochem 17:341–349

Beattie JR, Bell S, Moss BW (2004) A critical evaluation of Raman spectroscopy for the analysis of lipids: fatty acid methyl esters. Lipids 39:407–419

Beone GM, Carini F, Guidotti L, Rossi R, Gatti M, Fontanella MC, Cenci RM (2018) Potentially toxic elements in agricultural soils from the Lombardia region ofnorthern Italy. J Geochem Explor 190:436–452

Bissen M, Frimmel FH (2003) Arsenic—a review. Part I: occurrence, toxicity, speciation, mobility. Acta Hydrochim Hydrobiol 31:9–18

Blažková M (1996) Black triangle – most polluted part of mentral Europe. In: Rijtema PE, Eliáš V (eds) Regional approaches to water pollution in the environment, NATO ASI series, 2. Environment, vol 20. Kluwer Academic Publishers, Netherland, pp 227–249

Bonifacio E, Santoni S, Cudlín P, Zanini E (2008) Effect of dominant ground vegetation on soil organic matter quality in a declining mountain spruce forest of central Europe. Boreal Environ Res 13:113–120

Bray EE, Evans ED (1961) Distribution of n-paraffins as a clue to recognition of source beds. Geochim Cosmochim Acta 22:2–15

Bush RT, McInerney FA (2013) Leaf wax n-alkane distributions in and across modern plants: implications for paleoecology and chemotaxonomy. Geochim Cosmochim Acta 117:161–179

Bush RT, McInerney FA (2015) Influence of temperature and C4 abundance on n-alkane chain length distributions across the central USA. Org Geochem 79:65–73

Chumanová-Vávrová E, Cudlín O, Cudlín P (2015) Spatial and temporal patterns of ground vegetation dominants in mountain spruce forests damaged by sulphur air pollution (Giant Mountains, Czech Republic). Boreal Environ Res 20:620–636

Coward JL (2010) FTIR spectroscopy of synthesized racemic nonacosan-10-ol: a model compound for plant epicuticular waxes. J Biol Phys 36:405–425

Cranwell PA (1981) Diagenesis of free and bound lipids in terrestrial detritus deposited in a lacustrine sediment. Org Geochem 3:79–89

Diefendorf AF, Leslie AB, Wing SL (2015) Leaf wax composition and carbon isotopes vary among major conifer groups. Geochim Cosmochim Acta 170:145–156

Doherty SJ, Tighe MK, Wilson SC (2017) Evaluation of amendments to reduce arsenic and antimony leaching from co-contaminated soils. Chemosphere 174:208–217

Drda V (1994) SO_2 sources and their negative influence on the air quality in the Krkonoše and Jizerské hory Mts. with reference to the destruction of forest ecosystems. In: Annual report of the project PPZP MZP GA/78/93 reconstruction of forest ecosystems in the Krkonoše National Park. Office of the Krkonoše National Park, Vrchlabí, Czech Republic

Drissner D, Blum H, Tscherko D, Kandeler E (2007) Nine years of enriched CO_2 changes the function and structural diversity of soil microorganisms in a grassland. Eur J Soil Sci 58:260–269

Dubis EN, Dubis AT, Morzycki JW (1999) Comparative analysis of plant cuticular waxes using HATR FT-IR reflection technique. J Mol Struct 511–512:173–179

Edwards HGM, Farwell DW, Daffner L (1996) Fourier-transform Raman spectroscopic study of natural waxes and resins. Spectrochim Acta A 52:1639–1648

Gallet C, Keller C (1999) Phenolic composition of soil solutions: comparative study of lysimeter and centrifuge waters. Soil Biol Biochem 31:1151–1160

Gleixner G (2013) Soil organic matter dynamics: a biological perspective derived from the use of compound-specific isotopes studies. Ecol Res 28:683–695

Gocke M, Peth S, Wiesenberg GLB (2014) Lateral and depth variation of loess organic matter overprint related to rhizoliths — revealed by lipid molecular proxies and X-ray tomography. Catena 112:72–85

Graber ER, Tsechansky L (2010) Rapid one-step method for total fatty acids in soils and sediments. Soil Sci Soc Am J 74:42–50

Harmanescu M (2012) Comparative researches on two direct transmethylation without prior extraction methods for fatty acids analysis in vegetal matrix with low fat content. Chem Cent J 6:8

Hatcher PG, Spiker EC, Szverenyri M, Maciel GE (1983) Selective preservation: the origin of petroleum forming aquatic kerogen. Nature 305:498–501

He Y, Xiang Y, Zhou Y, Yang Y, Zhang J, Huang H, Shang C, Luo L, Gao J, Tang L (2018) Selenium contamination, consequences and remediation techniques in water and soils: a review. Environ Res 164: 288–301

Hejcman M, Dvořák I, Kociánová M, Pavlů V, Nezerková P, Vítek O, Rauch O, Jeník J (2006) Snow depth and vegetation pattern in a late-melting snowbed analyzed by GPS and GIS in the Giant Mountains, Czech Republic. Arct Antarct Alp Res 38:90–98

Heredia-Guerrero JA, Benítez JJ, Domínguez E, Bayer IS, Cingolani R, Athanassiou A, Heredia A (2014) Infrared and Raman spectroscopic features of plant cuticles: a review. Front Plant Sci 5:1–14

Hoffmann B, Kahmen A, Cernusak LA, Arndt SK, Sachse D (2013) Abundance and distribution of leaf wax n-alkanes in leaves of acacia and eucalyptus trees along a strong humidity gradient in northern Australia. Org Geochem 62:62–67

Christie WW, Han X (2010) Lipid analysis - isolation, separation, identification and lipidomic analysis, U.K. Oily Press, Bridgwater

Imperato M, Adamo P, Naimo D, Arienzo M, Stanzione D (2003) Spatial distribution of heavy metals in urban soils of Naples city. Environ Pollut 124:247–256

IUSS Working Group WRB (2007) World reference base for soil resources 2006, first update 2007, World Soil Resources Reports No. 103, FAO: Rome

Jansen B, Wiesenberg GLB (2017) Opportunities and limitations related to the application of plant-derived lipid molecular proxies in soil science. Soil 3:211–234

Jones RN, McKay AF, Sinclair RG (1952) Band progressions in the infrared spectra of fatty acids and related compounds. J Am Chem Soc 74:2575–2578

Kögel-Knabner I (2000) Analytical approaches for characterizing soil organic matter. Org Geochem 31:609–625

Koch K, Ensikat H-J (2008) The hydrophobic coatings of plant surfaces: epicuticular wax crystals and their morphologies, crystallinity and molecular self-assembly. Micron 39:759–772

Kolář T, Čermák P, Oulehle F, Trnka M, Štěpánek P, Cudlín P, Hruška J, Büntgen U, Rybníček M (2015) Pollution control enhanced spruce growth in the "Black Triangle" near the Czech–Polish border. Sci Total Environ 538:703–711

Kolattukudy PE (1970) Plant waxes. Lipids 5:259–275

LeRoux JH (1969) Fischer-Tropsch waxes: I. An infra-red method for the determination of crystallinity. J Appl Chem 19:3–42

Li X, Anderson BJ, Vogeler I, Schwendenmann L (2018) Long-chain n-alkane and n-fatty acid characteristics in plants and soil - potential to separate plant growth forms, primary and secondary grasslands? Sci Total Environ 645:1567–1578

Lin R, Ritz P (1993) Reflectance FTIR microspectroscopy of fossil algae contained in organic-rich shales. Appl Spectrosc 47:265–271

Locatelli M, Mocan A, Carradori S (2019) Innovative extraction techniques and hyphenated instrument configuration for complex matrices analysis. MDPI, Switzerland

Lu S, Russell AE, Hendra PJ (1998) The Raman spectra of high modulus polyethylene fibres by Raman microscopy. J Mater Sci 33:4721–4725

Maffei M, Badino S, Bossi S (2004) Chemotaxonomic significance of leaf wax n-alkanes in the Pinales (Coniferales). J Biol Res 1:3–19

Mäkelä MR, Marinović M, Nousiainen P, Liwanag AJM, Benoit I, Sipilä J, Hatakka A, de Vries RP, Hildén KS (2015) Aromatic metabolism of filamentous fungi in relation to the presence of aromatic compounds in plant biomass. Adv Appl Microbiol 91:63–137

McCauley A, Jones C, Olson-Rutz K (2017) Soil pH and organic matter. Nutrient Management Module No. 8, 4449-8, Montana State University/ extension

Merk S, Blum A, Riederer M (1998) Phase behaviour and crystallinity of plant cuticular waxes studied by Fourier transform infrared spectroscopy. Planta 204:44–53

Miller RO, Gavlak R, Horneck D (2013) Plant, soil and water reference methods for the Western Region. Western Rural Development Center, Corvallis

Mizera J, Řanda Z (2010) Instrumental neutron and photon activation analyses of selected geochemical reference materials. J Radioanal Nucl Chem 284:157–163

Movasaghi Z, Rehman S, Rehman I (2008) Fourier transform infrared (FTIR) spectroscopy of biological tissues. Appl Spectrosc Rev 43: 134–179

Naafs DFW, van Bergena PF, Boogerta SJ, de Leeuw JW (2004) Solvent-extractable lipids in an acid andic forest soil; variations with depth and season. Soil Biol Biochem 36:297–308

Neubert R, Rettig W, Wartewig S, Wegener M, Wienhold A (1997) Structure of stratum corneum lipids characterized by FT-Raman

spectroscopy and DSC. II. Mixtures of ceramides and saturated fatty acids. Chem Phys Lipids 89:3–14

Nierop KGJ, Naafs DFW, van Bergen PF (2005) Origin, occurrence and fate of extractable lipids in Dutch coastal dune soils along a pH gradient. Org Geochem 36:555–566

Norby RJ, Luo Y (2004) Evaluating ecosystem responses to rising atmospheric CO_2 and global warming in a multi-factor world. New Phytol 162:281–293

Otto A, Simpson MJ (2006) Sources and composition of hydrolysable aliphatic lipids and phenols in soils from western Canada. Org Geochem 37:385–407

Otto A, Shunthirasingham C, Simpson MJ (2005) A comparison of plant and microbial biomarkers in grassland soils from the Prairie Ecozone of Canada. Org Geochem 36:425–448

Parikh SJ, Goyne KW, Margenot AJ, Mukome FND, Calderon FJ (2014) Soil chemical insights provided through vibrational spectroscopy. Adv Agron 126:1–148

Peter M, Ayer F, Cudlín P, Egli S (2008) Belowground ectomycorrhizal communities in three Norway spruce stands with different degrees of decline in the Czech Republic. Mycorrhiza 18:157–169

Peters KE, Walters CC, Moldowan JM (2005) The biomarker guide. Cambridge University Press, Cambridge

Reimann C, Arnoldussen A, Englmaier P, Filzmoser P, Finne TE, Garrett RG, Koller F, Nordgulen Ø (2007) Element concentrations and variations along a 120 km long transect in South Norway e anthropogenic vs. geogenic vs. biogenic element sources and cycles. Appl Geochem 22:851–871

Riederer M, Matzke K, Ziegler F, Kögel-Knabner I (1993) Occurrence, distribution and fate of the lipid plant biopolymers cutin and suberin in temperate forest soils. Org Geochem 20:1063–1076

Rushdi AI, Oros DR, Al-Mutlaq KF, He D, Medeiros PM, Simoneit BRT (2016) Lipid, sterol and saccharide sources and dynamics in surface soils during an annual cycle in a temperate climate region. Appl Geochem 66:1–13

Sánchez-Rodas D, Alsioufi L, Sánchez de la Campa AM, González-Castanedo Y (2017) Antimony speciation as geochemical tracer for anthropogenic emissions of atmospheric particulate matter. J Hazard Mater 324:213–220

Scalan RS, Smith JE (1970) An improved measure of the odd-even predominance in the normal alkanes of sediment extracts and petroleum. Geochim Cosmochim Acta 34:611–620

Shoeneberger PJ, Wysocki DA, Benham EC, Broderson WD (2002) Field book for describing and sampling soils. < http://soils.usda.gov/technical/fieldbook/> (Accessed 12 April 2010)

Schäfer IK, Lanny V, Franke J, Eglinton TI, Zech M, Vysloužilová B, Zech R (2016) Leaf waxes in litter and topsoils along a European transect. Soil 2:551–564

Simoneit BRT (2005) A review of current applications of mass spectrometry for biomarker/molecular tracer elucidations. Mass Spectrom Rev 24:719–765

Sucharová J, Suchara I, Holá M, Reimann C, Boyd R, Filzmoser P, Englmaier P (2011) Linking chemical elements in forest floor humus (Oh-horizon) in the Czech Republic to contamination sources. Environ Pollut 159:1205–1214

Swalen JD, Allara DL, Andrade JD, Chandross EA, Garoff S, Israelachvili J, McCarthy TJ, Murray R, Pease RF, Rabolt JF, Wynne KJ, Yu H (1987) Molecular monolayers and films. Langmuir 3:932–950

Ussiri DAN, Johnson CE (2003) Characterization of organic matter in a northern hardwood forest soil by 13C NMR spectroscopy and chemical methods. Geoderma 111:123–149

Vacek S, Bílek L, Schwarz O, Hejcmanová P, Mikeska P (2013) Effect of air pollution on the health status of spruce stands. A case study in the Krkonoše Mountains, Czech Republic. Mt Res Dev 33:40–50

Vávrová E, Cudlín O, Vavříček D, Cudlín P (2009) Ground vegetation dynamics in mountain spruce (Picea abies (L.) Karsten) forests recovering after air pollution stress impact. Plant Ecol 205:305–321

Wiesenberg GLB, Schwark L, Schmidt MWI (2005) Extractable lipid contents and colour in particle-size separates and bulk arable soils. Eur J Soil Sci 57:634–543

Yelpatyevsky PV, Arghanova VS, Lutsenko TN (1995) Heavy metals in polluted ecosystem of an oak forest. Sci Total Environ 162:13–18

Zech M, Buggle B, Leiber K, Marković S, Glaser B, Hambach U, Huwe B, Stevens T, Sümegi P, Wiesenberg GLB, Zöller L (2009) Reconstructing Quaternary vegetation history in the Carpathian Basin, SE Europe, using n-alkane biomarkers as molecular fossils: problems and possible solutions, potential and limitations. J Quat Sci 58:148–155

Zerbi G, Magni R, Gussoni M, Moritz KH, Bigotto A, Dirlikov S (1981) Molecular mechanics for phase transition and melting of n-alkanes: a spectroscopic study of molecular mobility of solid n-nonadecane. J Chem Phys 75:3175–3194

Zhou Q, Teng Y, Liu Y (2017) A study on soil-environmental quality criteria and standards of arsenic. Appl Geochem 77:158–166